Pergamon

J. Mech. Phys. Solids, Vol. 44, No. 10, pp. 1621–1648, 1996
Copyright © 1996 Elsevier Science Ltd
Printed in Great Britain. All rights reserved
0022–5096/96 $15.00 + 0.00

PII S0022–5096(96)00035–X

CRACK TIP FIELDS IN STRAIN GRADIENT PLASTICITY

Z. CEDRIC XIA* and JOHN W. HUTCHINSON

Division of Applied Sciences, Harvard University, Cambridge, MA 02138, U.S.A.

(*Received* 28 *September* 1995; *in revised form* 29 *December* 1995)

ABSTRACT

Solutions are presented for mode I and mode II crack tip fields for plane strain deformations of an elastic–plastic solid whose constitutive behavior depends on both strains and strain gradients. The constitutive law is the simplest generalization of the J_2 deformation theory of plasticity to include strain gradient effects. Only one new constitutive parameter enters, a length parameter characterizing the scale over which gradient effects become important. The formulation is cast within the framework of coupled stress theory. Crack tip solutions are obtained which display the transition from the HRR fields, governing behavior in an intermediate region with the plastic zone, to the dominant fields at the tip. The dominant fields are obtained in closed form, and finite element methods have been used to produce the solution over the entire field. Some of the difficulties encountered in arriving at an accurate numerical scheme are detailed. Implications of the solutions for fracture are discussed, as are avenues for further research. Copyright © 1996 Elsevier Science Ltd

Keywords: A, crack tip plasticity, A, fracture, B, constitutive behavior, C, finite elements, C, asymptotic analysis.

1. INTRODUCTION

Attempts to link macroscopic fracture behavior to atomistic fracture processes in ductile metals are frustrated by the inability of conventional plasticity theories to adequately model stress–strain behavior at the small scales required in crack tip models. Adding to the complications of the atomistic separation processes and interactions of individual dislocations with the crack tip, is the complication of an intermediate region lying between the tip and the outer plastic zone within which stresses are almost certainly much higher than implied by conventional plasticity theory. This discrepancy does not appear to be an issue for the ductile mechanism of fracture associated with void nucleation, growth, and coalescence, because the scale of the ductile fracture process is usually of the order of 10 μm or more and the largest crack tip stresses are never more than about 3–5 times the tensile flow stress. However, for atomistic fracture mechanisms, conventional plasticity is unable to explain how stresses at a crack tip can reach levels necessary to bring about atomic decohesion.

An increasing body of experimental evidence points to the fact that metals require significantly higher stresses to induce plastic deformation at micrometer and submicrometer scales than at larger macroscopic scales. Indentation tests on several

* Current address: Scientific Research Laboratories, Ford Motor Company, Dearborn, MI 48121, U.S.A.

metals (Stelmashenko *et al.*, 1993; Ma and Clarke, 1995; Poole *et al.*, 1995) display increases of hardness by as much as three time the macroscopic hardness for indentations diminishing in size from 10s of micrometers to a fraction of a micrometer. The scale in these tests is such that the indentation is still much larger than the average dislocation spacing, and a continuum description of plasticity remains imperative if the deformation is to be modeled. Within a continuum formulation, the strong size dependence is introduced through strain gradient effects. The most compelling evidence so far for this approach comes from the thin wire tests of Fleck *et al.* (1994). For copper wires ranging in radius from 6–60 μm, there is little evidence of any size dependence in the uniaxial tension for which strain gradients are absent. In torsion, however, which imposes a deformation gradient on the wire, there is a strong size effect with thinner wires displaying significantly higher effective shear stress–strain behavior than thicker wires.

The strain gradient effect introduced by Fleck *et al.* (1994) was related to the generation of geometrically necessary dislocations which accompany almost all deformations involving strain gradients. The total dislocation density is taken to be proportional to the sum of the plastic strain and the strain gradient (i.e. $\rho \propto \varepsilon + l\,\partial\varepsilon/\partial x$) in a manner prescribed in the next section. The only new constitutive parameter in the theory is the length parameter l. The torsion tests referred to above indicated $l = 4$ μm for the particular copper comprising the wires. Strain gradients become large in the vicinity of a crack tip, and a theory incorporating strain gradient effects is expected to produce stress and strain distributions which are modified from the predictions of a conventional plasticity theory within distances from the tip of the order of l. The aim of this paper is to provide these near-tip stress and strain distributions for a particular strain gradient theory.

2. GOVERNING EQUATIONS AND PROBLEM STATEMENT

2.1. *Field equations for strain gradient plasticity*

The deformation theory of strain gradient plasticity detailed by Fleck and Hutchinson (1993) is used in the present study. The solid is taken to be homogeneous and isotropic with an energy density W which depends on scalar invariants of the strain tensor $\boldsymbol{\varepsilon}$ and the deformation curvature tensor $\boldsymbol{\chi}$. Coupled stress theory is invoked to complete the characterization. The stress quantities which are work conjugate to the two strain quantities are the symmetric part of the Cauchy stress $\boldsymbol{\sigma}$ and the unsymmetric coupled stress $\mathbf{m}$. The following small strain formulation represents the simplest generalization of the widely-used J_2 deformation theory of plasticity.

With u_i as the displacement vector, ε_{ij} as the linearized strain tensor, $\theta_i \equiv \frac{1}{2} e_{ijk} u_{k,j}$ as the linearized rotation vector, let the linearized curvature tensor be $\chi_{ij} = \theta_{i,j}$ and note that it can be expressed in terms of the strain gradients as $\chi_{ij} = e_{ikl}\varepsilon_{jl,k}$. The curvature tensor $\boldsymbol{\chi}$ is an unsymmetric deviatoric tensor. Let $\varepsilon_m = \varepsilon_{kk}/3$, $\varepsilon'_{ij} = \varepsilon_{ij} - \varepsilon_m \delta_{ij}$ and $\varepsilon_e \equiv \sqrt{\frac{2}{3}\varepsilon'_{ij}\varepsilon'_{ij}}$. The invariant of $\boldsymbol{\chi}$ used to form the dependence on strain gradients is $\chi_e \equiv \sqrt{\frac{2}{3}\chi_{ij}\chi_{ij}}$. Additional invariants of the strain tensor are not taken into account in this formulation. Certain strain gradients make no contribution to χ_e, an example

being an irrotational deformation field (i.e. $\theta_i = 0$). The two invariants, ε_e and χ_e, are combined into a single effective strain quantity according to

$$E^2 \equiv \varepsilon_e^2 + l^2 \chi_e^2, \tag{2.1}$$

where l is a material length quantity which becomes the sole additional constitutive parameter in the theory. The physical basis for combining the terms in this manner is discussed in Fleck *et al.* (1994). In the simplest interpretation, ε_e is regarded as a measure of the density of statistically stored dislocations and χ_e is a measure of the density of geometrically necessary dislocations produced by the strain gradients. Thus, E is regarded as a measure of the total dislocation density. The energy density for the deformation solid is postulated to be

$$W(E, \varepsilon_m) = w(E) + \tfrac{1}{2}\kappa \varepsilon_m^2, \tag{2.2}$$

where the elastic part of the strain energy due to the deviatoric strains is included in w, and κ is the bulk modulus of the solid. For an incompressible material, the second term in (2.2) vanishes.

With σ_{ij} as the symmetric part of the stress tensor, $\sigma_m = \sigma_{kk}/3$, $s_{ij} = \sigma_{ij} - \sigma_m \delta_{ij}$, and with m_{ij} as the unsymmetric, deviatoric couple stress tensor,

$$\delta W = \sigma_{ij}\, \delta \varepsilon_{ij} + m_{ij}\, \delta \chi_{ji} = s_{ij}\, \delta \varepsilon'_{ij} + m_{ij}\, \delta \chi_{ji} + \sigma_m\, \delta \varepsilon_m, \tag{2.3}$$

where

$$\sigma_{ij} = \frac{\partial W}{\partial \varepsilon_{ij}}, \quad m_{ij} = \frac{\partial W}{\partial \chi_{ji}}, \quad \text{or} \quad s_{ij} = \frac{\partial w}{\partial \varepsilon'_{ij}}, \quad m_{ij} = \frac{\partial w}{\partial \chi_{ji}}, \quad \sigma_m = \kappa \varepsilon_m. \tag{2.4}$$

An effective stress can be defined as

$$\Sigma^2 = \sigma_e^2 + l^{-2} m_e^2, \tag{2.5}$$

where $\sigma_e = \sqrt{3 s_{ij} s_{ij}/2}$ and $m_e = \sqrt{3 m_{ij} m_{ij}/2}$. The effective stress and strain are related by

$$\Sigma = \partial w / \partial E \tag{2.6}$$

from which it follows that

$$s_{ij} = \frac{2}{3}\frac{\Sigma}{E}\varepsilon'_{ij} \quad \text{and} \quad m_{ij} = \frac{2}{3} l^2 \frac{\Sigma}{E} \chi_{ji}. \tag{2.7}$$

The focus of the present study of crack tip fields will be on behavior within the plastic zone where stresses have exceeded yield. Within the plastic range, the solid will be represented by the power law relation

$$w = \frac{n}{n+1} \sigma_0 \varepsilon_0 \left(\frac{E}{\varepsilon_0}\right)^{(n+1)/n} \quad \text{such that} \quad \frac{\Sigma}{\sigma_0} = \left(\frac{E}{\varepsilon_0}\right)^{1/n}. \tag{2.8}$$

As in the conventional formulation, σ_0 is identified with a measure of the tensile yield stress and ε_0 is the associated elastic tensile strain at that stress. When strain gradients

are small (i.e. $l\chi_e \ll \varepsilon_e$), the above relation reduces to the J_2 deformation theory of plasticity for a power law solid.

A principle of virtual work is postulated, thereby embedding the theory within the framework of coupled stress theory [Fleck *et al.* (1993), c.f. Koiter (1964) for coupled stress theory]. Let τ_{ij} be the anti-symmetric part of the stress such that the traction vector acting on a surface element with unit normal n_i is $T_j = (\sigma_{ij} + \tau_{ij})n_i$, and let $q_j = m_{ij}n_i$ be the coupled stress traction vector. The principle of virtual work statement for all admissible variations δu_i is

$$\int_S [T_i\,\delta u_i + q_i\,\delta\theta_i]\,\mathrm{d}S = \int_V [\sigma_{ij}\,\delta\varepsilon_{ij} + m_{ij}\,\delta\chi_{ji}]\,\mathrm{d}V. \tag{2.9}$$

The associated equilibrium equations in the absence of body forces or couples are

$$\sigma_{ji,j} + \tau_{ji,j} = 0 \quad \text{and} \quad \tau_{jk} = -\tfrac{1}{2}e_{ijk}m_{pi,p} \tag{2.10}$$

If desired, the anti-symmetric part of the stress, τ_{ij}, can be eliminated in the field equations in favor of the gradients of the coupled stresses using the second equation in (2.10). Since these components will prove to be significant, we will retain them as explicit variables. Under conditions that W is convex, principles of minimum potential energy and complementary energy can be constructed (Fleck *et al.*, 1993). Versions of these principles will be used in formulating the numerical solution methods.

2.2. *Formulation of the problem for the crack tip fields*

Pure mode I and mode II problems in plane strain will be considered with non-zero displacements $u_1(x_1, x_2)$ and $u_2(x_1, x_2)$. The only non-zero rotation component is θ_3 with its associated component of moment traction q_3. The list of non-zero stress and strain quantities is: σ_{11}, σ_{22}, σ_{33}, $\sigma_{12} = \sigma_{21}$, $\tau_{12} = -\tau_{21}$, ε_{11}, ε_{22}, ε_{12}, ε_{11}, χ_{31}, χ_{32}, m_{13} and m_{23}. The crack tip is located at the origin and the crack lies along the negative x_1 axis, as shown in Fig. 1. The following generalization of Rice's (1968) path-independent J-integral exists for the deformation theory solid

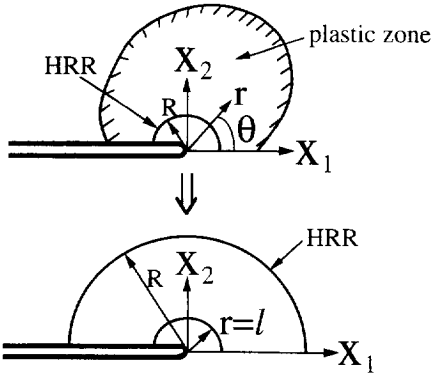

Fig. 1. Asymptotic crack tip geometry for plane strain problems.

$$J = \int_C (Wn_1 - T_i u_{i,1} - q_i \theta_{,1}) \, ds, \tag{2.11}$$

where C is any contour circling the crack tip originating on the lower crack surface and ending on the upper crack surface with s as the distance along the contour. When the force and moment tractions vanish on the crack surfaces, J has the same value for all such contours C. The value J will be used as the amplitude measure in what follows. In small-scale yielding, $J = (1-\nu^2)K^2/E$, where K is either the mode I or mode II elastic stress intensity factor, E is Young's modulus and ν is Poisson's ratio. However, for the problem posed below there is no need to invoke small-scale yielding.

As previously noted, the above formulation reduces to conventional deformation theory for a power-law solid when $l = 0$. The singular crack tip fields in that limit are the HRR fields (Hutchinson, 1968; Rice and Rosengren, 1968)

$$u_i = \varepsilon_0 \left(\frac{J}{\sigma_0 \varepsilon_0 I_n r} \right)^{n/(n+1)} r \tilde{u}_i(\theta, n),$$

$$\varepsilon_{ij} = \varepsilon_0 \left(\frac{J}{\sigma_0 \varepsilon_0 I_n r} \right)^{n/(n+1)} \tilde{\varepsilon}_{ij}(\theta, n) \quad \sigma_{ij} = \sigma_0 \left(\frac{J}{\sigma_0 \varepsilon_0 I_n r} \right)^{1/(n+1)} \tilde{\sigma}_{ij}(\theta, n), \tag{2.12}$$

where r and θ are polar coordinates centered at the tip. The functions of n and θ, $\tilde{u}$, $\tilde{\sigma}$, and $\tilde{\varepsilon}$, depend on whether mode I or mode II holds, as does the function of n, I_n. These functions are tabulated and available in the report by Symington *et al.* (1988).

According to the HRR distribution (2.12), strain gradients are unbounded at the crack tip, varying as $r^{-(2n+1)/(n+1)}$. The zone in which strain gradient effects become important is located at the crack tip and is surrounded by the HRR field. Formally, with R_p as the size of the plastic zone and with J sufficiently large such that $R_p \gg l$, one can pose the asymptotic crack tip problem depicted schematically in Fig. 1 wherein the solution to the complete strain gradient problem is required to approach (2.12) in the outer field for $r/l \gg 1$. It will be seen that the departures of the complete solution from the HRR solution become significant when r/l is of the order of unity. In carrying out the numerical analysis described in the next section, we impose conditions on the outer radius R of the meshed region using u_i in (2.12) to specify the displacements and rotation, with R/l chosen to be sufficiently large to ensure that the outer field does approach the HRR limit. The asymptotic problem of Fig. 1 can be meaningfully posed for the limit of an elastically incompressible material ($\kappa \to \infty$), but for numerical purposes it is useful to keep κ finite.

The focus in this paper is on the influence of strain gradient effects near the crack tip within the regime of load and parameters such that the present small strain formulation is valid. We proceed by anticipating that such a regime does exist, and return to the issue after the small strain solution has been produced to give precise conditions which ensure that large strain effects, such as crack tip blunting, do not invalidate the small strain assumptions.

The path independence of the J-integral in (2.11) allows one to draw some conclusions about the asymptotic behavior of the solution as $r \to 0$. As in the conventional theory, (2.11) suggests that $W \to f(\theta)/r$ as $r \to 0$, and it will be seen that this is indeed

the case. Some of the conclusions about the distributions of the stress and strain quantities which follow from this asymptotic behavior for W are subtle and not easy to anticipate. Elastic compressibility does not affect the most singular fields, and without loss of generality we will take $\kappa \to \infty$ in the following discussion. As the first step, suppose that the strains vary as r^{-s} as the tip is approached such that $\varepsilon_e \to r^{-s}$. Assuming the displacements generating these strains are not irrotational, then χ_e would behave like r^{-s-1} as $r \to 0$, and the strain gradient terms would dominate W as the tip is approached. In fact, we find that the dominant fields at the tip are irrotational (i.e. have $\theta_3 = 0$ and, therefore, give no contribution to χ_e to lowest order) such that the strains and not the curvatures are dominant at the crack tip. Then, by (2.1), (2.8) and the requirement that $W \to r^{-1}$, one is led to the conclusion that $s = n/(n+1)$ with $\varepsilon_e \to r^{-n/(n+1)}$ and $\sigma_e \to r^{-1/(n+1)}$, as is the case for the HRR fields. The one non-zero nonsymmetric stress component, τ_{12}, has the same singularity as the other stress components. Explicit closed-form expressions for the dominant fields will be obtained which agree with a particular limit obtained by Huang *et al.* (1995).

In general, the solution in plane strain, mode I and mode II can be written as

$$[\varepsilon_{ij}, l\chi_{ij}] = \varepsilon_0 \left(\frac{J}{\sigma_0 \varepsilon_0 I_n r}\right)^{n/(n+1)} \left[\hat{\varepsilon}_{ij}\left(\theta, \frac{r}{l}, n\right), \hat{\chi}_{ij}\left(\theta, \frac{r}{l}, n\right)\right],$$

$$[\sigma_{ij}, l^{-1} m_{ij}, \tau_{ij}] = \sigma_0 \left(\frac{J}{\sigma_0 \varepsilon_0 I_n r}\right)^{n/(n+1)} \left[\hat{\sigma}_{ij}\left(\theta, \frac{r}{l}, n\right), \hat{m}_{ij}\left(\theta, \frac{r}{l}, n\right), \hat{\tau}_{ij}\left(\theta, \frac{r}{l}, n\right)\right]. \tag{2.13}$$

Based on the observations outlined above, it will be argued that the dominantly singular crack tip fields are such that $\hat{\varepsilon}_{ij}$, $\hat{\sigma}_{ij}$, and $\hat{\tau}_{ij}$ are all finite as $r/l \to 0$, while $\hat{\chi}_{ij}$ and $\hat{m}_{ij}$ approach zero. Numerical results will be presented in Section 4 for these dimensionless quantities for r/l ranging from values which are small compared to 1 to values which are sufficiently large that the HRR solution is approached. In the outer field where the HRR solution is approached, $\hat{\varepsilon}_{ij}$ and $\hat{\sigma}_{ij}$, respectively, approach $\tilde{\varepsilon}_{ij}$ and $\tilde{\sigma}_{ij}$ defined by (2.12). As $r/l \to 0$, the dominant singular fields given in Section 5 are approached.

3. FINITE ELEMENT FORMULATION

In this section, several finite elements will be specified for the deformation theory of strain gradient plasticity outlined in the last section. The potential energy $P(\mathbf{u})$ is given by (Fleck and Hutchinson, 1993)

$$P(\mathbf{u}) = \int_V \left\{ w(\boldsymbol{\varepsilon}, \boldsymbol{\chi}) + \frac{1}{2}\kappa \varepsilon_m^2 \right\} \mathrm{d}V - \int_{S_T} (T_i^0 u_i + q_i^0 \theta_i)\, \mathrm{d}S, \tag{3.1a}$$

where $w(\boldsymbol{\varepsilon}, \boldsymbol{\chi})$ is defined in (2.8), and the surface integral is taken over that part S_T of the surface of the body over which T_i and q_i are prescribed. The principle of minimum potential energy states that among all the kinematically admissible displacement fields

$\mathbf{u}$, the actual displacement field will render $P(\mathbf{u})$ an absolute minimum, provided w is strictly convex in $\boldsymbol{\varepsilon}$ and $\boldsymbol{\chi}$. The associated variational statement is

$$\delta P(\mathbf{u}) = 0. \tag{3.1b}$$

For finite element formulations based on the principle of minimum potential energy, admissibility conditions dictate continuity of rotations, θ_i, requiring elements which have C_1 continuity in displacements, u_i. Alternatively, the finite element scheme can be formulated based on other mixed variational statements, relaxing the C_1 continuity requirement. We have found that the choice of element for gradient plasticity is complicated and, in particular, quite sensitive to details of the constitutive relation. So that others will not have to repeat our steps in element development, we have chosen to give a reasonably systematic presentation of the elements we have tried, indicating our experience with each one. A displacement-based C_1 element for anti-plane deformation will first be discussed, followed by its extension to the plane strain case. Difficulties with this class of element will be noted. Other elements are then explored for plane strain deformation based on mixed variational statements. The element used to carry out the present crack tip calculations is indicated at the end of Section 3.2, and readers wishing to bypass details about the choice of finite element may want to skip directly to that section.

One important consideration in finite element formulation of current strain gradient plasticity is the continuity of rotations θ_i while imposing $\theta_i \equiv \frac{1}{2} e_{ijk} u_{k,j}$. If a general couple-stress theory is adopted where the rotations θ_i are treated as independent of displacements u_i, as proposed originally by the Cosserat brothers (Cosserat and Cosserat, 1909), the procedure for finite element formulation will be greatly simplified. It has been used by de Borst (1993) and others to study localization problems, which is different from the current study.

3.1. *A* C_1 *element for anti-plane deformation and its extension to the plane strain case*

In anti-plane deformation, the only non-vanishing displacement quantity is $u \equiv u_3$. The rotations are related to u by

$$\theta_1 = \tfrac{1}{2} u_{,y}, \quad \theta_2 = -\tfrac{1}{2} u_{,x}, \quad \text{and} \quad \theta_3 = 0. \tag{3.2}$$

To develop a C_1 element for the strain gradient plasticity in anti-plane shear, one can exploit the similarity with the bending of plates where continuity of the normal displacement and its first partial derivatives is required. Extensive research into finite element formulations for plates in the past several decades has produced several elements which perform well in applications. The C_1 elements selected for discussion are similar to one given in Zienkiewicz and Taylor (1989b), whose notation and formalism are adopted here.

Consider a triangular element with corner nodes in the (x, y) plane. This element has three nodal variables at each node, namely the displacement u and its two first derivatives $u_{,x}$ and $u_{,y}$. As is common in finite element formulations, the displacement field within one element will be given by a listing of the nodal variables, now totaling nine

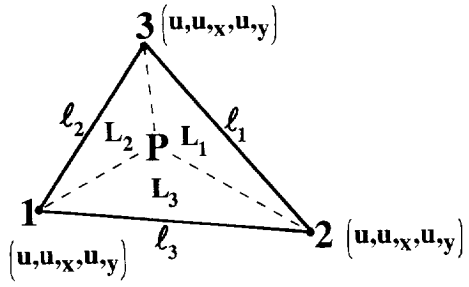

Fig. 2. A 3-noded displacement-based C_1 element for anti-plane deformation.

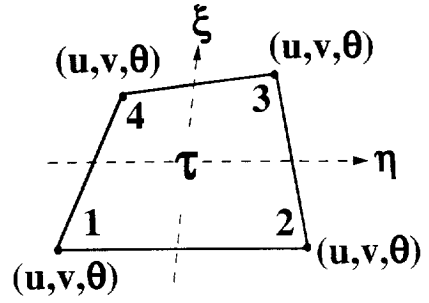

Fig. 3. A 4-noded hybrid element for plane strain deformation.

$$\mathbf{a} = \begin{Bmatrix} \mathbf{a}_1 \\ \mathbf{a}_2 \\ \mathbf{a}_3 \end{Bmatrix}, \quad \text{where} \quad \mathbf{a}_i = \begin{Bmatrix} u \\ u_{,x} \\ u_{,y} \end{Bmatrix}_i. \tag{3.3}$$

Since this element has three nodes and nine degrees of freedom (DOF), it will be designated here as N3U9 for convenience.

Following Zienkiewicz and Taylor (1989b), a polynomial expression utilizing area coordinates is used to define the shape functions in terms of the nine nodal variables. As shown in Fig. 2, the position of point P is determined by its three area coordinates L_1, L_2, and L_3, where L_1 = area P23/area 123, etc. Area coordinates are a natural choice for formulating triangular elements (Zienkiewicz and Taylor, 1989a, b). Now assume that the displacement field within one element can be approximated by

$$u = \alpha_1 L_1 + \alpha_2 L_2 + \alpha_3 L_3 + \alpha_4 L_1 L_2 + \alpha_5 L_2 L_3 + \alpha_6 L_3 L_1 + \alpha_7 L_1^2 L_2 + \alpha_8 L_2^2 L_3 + \alpha_9 L_3^2 L_1, \tag{3.4}$$

where the α_is are free parameters to be determined. By relating the nine α_is to the nine nodal variables, we find, after some algebra, that (3.4) can be re-written as

$$u = \sum_{i=1}^{3} \mathbf{N}_i \mathbf{a}_i, \tag{3.5}$$

$$N_i^{\mathrm{T}} = \begin{Bmatrix} N_i^1 \\ N_i^2 \\ N_i^3 \end{Bmatrix} = \begin{Bmatrix} 3L_i^2 - 2L_i^3 - 2L_iL_jL_k \\ -c_j(L_i^2L_k + L_iL_jL_k) + c_kL_i^2L_j \\ b_j(L_i^2L_k + L_iL_jL_k) - b_kL_i^2L_j \end{Bmatrix}, \tag{3.6}$$

where

$$b_i = y_j - y_k, \quad c_i = x_k - x_j \tag{3.7}$$

and i, j, k are the cyclic permutations of 1, 2, 3.

For anti-plane deformation, the generalized strain vector $\mathbf{E}$ is given in terms of nodal variables by

$$\mathbf{E} \equiv \begin{Bmatrix} \gamma_x \\ \gamma_y \\ \chi_{11} \\ \chi_{12} \\ \chi_{21} \\ \chi_{22} \end{Bmatrix} = \begin{Bmatrix} \sum_{i=1}^{3} \mathbf{N}_{i,x}\mathbf{a}_i \\ \sum_{i=1}^{3} \mathbf{N}_{i,y}\mathbf{a}_i \\ \frac{1}{2}\sum_{i=1}^{3} \mathbf{N}_{i,xy}\mathbf{a}_i \\ \frac{1}{2}\sum_{i=1}^{3} \mathbf{N}_{i,yy}\mathbf{a}_i \\ -\frac{1}{2}\sum_{i=1}^{3} \mathbf{N}_{i,xx}\mathbf{a}_i \\ -\frac{1}{2}\sum_{i=1}^{3} \mathbf{N}_{i,xy}\mathbf{a}_i \end{Bmatrix} = \mathbf{Ba}, \tag{3.8}$$

where $\mathbf{B}$ is the strain shape function.

The corresponding generalized stress vector $\mathbf{\Sigma}$ is defined as

$$\mathbf{\Sigma} \equiv \{\tau_x, \tau_y, m_{11}, m_{21}, m_{12}, m_{22}\}^T, \tag{3.9}$$

where

$$\sum_i = \frac{\partial w(\varepsilon, \chi)}{\partial E_i}. \tag{3.10}$$

With shape functions given above and the principle of minimum potential energy as the basis, the formulation of finite element equations follows the standard pattern, and will not be documented here. It was found that volume integrals could be evaluated with sufficient accuracy using three-point numerical quadrature. The element passes the patch test, and performs quite well on the anti-plane shear problem. An independent study of the mode III crack problem within the framework of strain gradient plasticity, using this and other similar elements, will be published elsewhere by Shiermeier (1996). There are important differences between the form of the singularity in mode III and that in modes I and II.

The above element, N3U9, as well as other elements which will be introduced later

in this paper, was ported into the commercial finite element package ABAQUS through its user-defined element capability.

A modification of N3U9 derived by Specht (1988) has also been implemented. This modified element uses three fourth-order terms in place of the three cubic terms in (3.4), resulting in a new displacement field given by

$$\begin{aligned} u = {} & \alpha_1 L_1 + \alpha_2 L_2 + \alpha_3 L_3 + \alpha_4 L_1 L_2 + \alpha_5 L_2 L_3 + \alpha_6 L_3 L_1 \\ & + \alpha_7 \{L_1^2 L_2 + \tfrac{1}{2} L_1 L_2 L_3 [3(1-\mu_3)L_1 - (1+3\mu_3)(L_2 - L_3)]\} \\ & + \alpha_8 \{L_2^2 L_3 + \tfrac{1}{2} L_1 L_2 L_3 [3(1-\mu_1)L_2 - (1+3\mu_1)(L_3 - L_1)]\} \\ & + \alpha_9 \{L_3^2 L_1 + \tfrac{1}{2} L_1 L_2 L_3 [3(1-\mu_2)L_3 - (1+3\mu_2)(L_1 - L_2)]\}, \end{aligned} \tag{3.11}$$

where

$$\mu_1 = \frac{l_3^2 - l_2^2}{l_1^2} \quad \mu_2 = \frac{l_1^2 - l_3^2}{l_2^2} \quad \mu_3 = \frac{l_2^2 - l_1^2}{l_3^2} \tag{3.12}$$

and l_1, l_2, l_3 are lengths of corresponding triangle sides as indicated in Fig. 2.

Although this element is claimed to be one of the best in its class for plate bending, it does not give adequate results for the anti-symmetric stress quantities τ_{ij} in our strain gradient applications, which are computed from (2.10).

The extension of the element N3U9 to plane strain deformation is straightforward. Denote the two non-zero displacement components by $u = u_1$ and $v = u_2$. Accordingly, the element will now have six nodal variables at each node, namely,

$$\mathbf{a}_i = \{u \quad u_{,x} \quad u_{,y} \quad v \quad v_{,x} \quad v_{,y}\}_i^{\mathrm{T}}, \tag{3.13}$$

totaling 18 DOFs for one element. This element is thus denoted as N3U18.

The shape functions take the same forms as given in (3.4)–(3.7), except now for both u and v. The generalized strain vector $\mathbf{E}$ for plane strain deformation reads,

$$\mathbf{E} = \begin{Bmatrix} e_x \\ e_y \\ e_z \\ \gamma_{xy} \\ \chi_x \\ \chi_y \end{Bmatrix} = \sum_{i=1}^{3} \begin{Bmatrix} \frac{2}{3}N^1_{i,x} & \frac{2}{3}N^2_{i,x} & \frac{2}{3}N^3_{i,x} & -\frac{1}{3}N^1_{i,y} & -\frac{1}{3}N^2_{i,y} & -\frac{1}{3}N^3_{i,y} \\ -\frac{1}{3}N^1_{i,x} & -\frac{1}{3}N^2_{i,x} & -\frac{1}{3}N^3_{i,x} & \frac{2}{3}N^1_{i,y} & \frac{2}{3}N^2_{i,y} & \frac{2}{3}N^3_{i,y} \\ -\frac{1}{3}N^1_{i,x} & -\frac{1}{3}N^2_{i,x} & -\frac{1}{3}N^3_{i,x} & -\frac{1}{3}N^1_{i,y} & -\frac{1}{3}N^2_{i,y} & -\frac{1}{3}N^3_{i,y} \\ N^1_{i,y} & N^2_{i,y} & N^3_{i,y} & N^1_{i,x} & N^2_{i,x} & N^3_{i,x} \\ -\frac{1}{2}N^1_{i,xy} & -\frac{1}{2}N^2_{i,xy} & -\frac{1}{2}N^3_{i,xy} & \frac{1}{2}N^1_{i,xx} & \frac{1}{2}N^2_{i,xx} & \frac{1}{2}N^3_{i,xx} \\ -\frac{1}{2}N^1_{i,yy} & -\frac{1}{2}N^2_{i,yy} & -\frac{1}{2}N^3_{i,yy} & \frac{1}{2}N^1_{i,xy} & \frac{1}{2}N^2_{i,xy} & \frac{1}{2}N^3_{i,xy} \end{Bmatrix} \times \begin{Bmatrix} u_i \\ (u_{,x})_i \\ (u_{,y})_i \\ v_i \\ (v_{,x})_i \\ (v_{,y})_i \end{Bmatrix} = \mathbf{Ba}, \tag{3.14}$$

where $\mathbf{B}$ is the strain shape function. The corresponding generalized stress vector $\mathbf{\Sigma}$ is

$$\boldsymbol{\Sigma} \equiv \{\sigma_x, \sigma_y, \sigma_z, \sigma_{xy}, m_x, m_y\}^T. \tag{3.15}$$

The volumetric strain ε_m is related to the nodal variables by

$$\varepsilon_m = \sum_{i=1}^{3} \{N^1_{i,x} \quad N^2_{i,x} \quad N^3_{i,x} \quad N^1_{i,y} \quad N^2_{i,y} \quad N^3_{i,y}\}\mathbf{a}_i \tag{3.16}$$

with the hydrostatic stress p given by $p = \kappa\varepsilon_m$.

The finite element formulation for N3U18 is again based on the principle of minimum potential energy (3.1), and follows the standard procedure. Integration of the contribution of w to the strain energy is evaluated using three-point numerical quadrature. One-point reduced integration is used to evaluate the volumetric contribution to the strain energy, thereby avoiding possible locking phenomena in case the solid is incompressible or nearly incompressible (Zienkiewicz and Taylor, 1989a).

This element passes the patch test, performs well for both linear solids with couple stresses and conventional elastic–plastic solids (i.e. the present class of solids in either the linear limit or in the nonlinear case with $l = 0$). However, it fails to produce adequate results for the hydrostatic stress when applied to calculate crack tip fields for the general case—a phenomenon commonly encountered when developing new finite elements for incompressible or nearly incompressible solids. The performance difference observed for $l = 0$ and $l \neq 0$ strongly suggests that the performance of a given element is closely tied to the constitutive behavior, as borne out for other elements developed in this study.

To overcome the difficulty associated with the locking phenomena, two other variational statements have been used as the basis for the finite element formulation. One treats the hydrostatic stress p as an additional independent variable. It reads

$$\Pi(\mathbf{u}, p) = \int_V \left\{ w(\boldsymbol{\varepsilon}, \boldsymbol{\chi}) + \frac{1}{2\kappa}p^2 \right\} \mathrm{d}V + \int_V p\left(\varepsilon_{\mathrm{m}} - \frac{p}{\kappa}\right)\mathrm{d}V - \int_{S_T} (T_i^0 u_i + q_i^0 \theta_i)\,\mathrm{d}S \tag{3.17a}$$

with

$$\delta\Pi(\mathbf{u}, p) = 0. \tag{3.17b}$$

Another is modified from Simo *et al.* (1985) where both the hydrostatic stress p and the volumetric strain ε_{v} are independent variables in addition to the displacements. It has the form

$$\Pi(\mathbf{u}, p, \varepsilon_{\mathrm{v}}) = \int_V \left\{ w(\boldsymbol{\varepsilon}, \boldsymbol{\chi}) + \frac{1}{2}\kappa\varepsilon_{\mathrm{v}}^2 \right\} \mathrm{d}V + \int_V p(\varepsilon_{\mathrm{m}} - \varepsilon_{\mathrm{v}})\,\mathrm{d}V - \int_{S_T} (T_i^0 u_i + q_i^0 \theta_i)\,\mathrm{d}S \tag{3.18a}$$

with

$$\delta\Pi(\mathbf{u}, p, \varepsilon_{\mathrm{v}}) = 0. \tag{3.18b}$$

In this formulation, the volumetric strain given by (3.16) is enforced in an averaged sense, as indicated in the second term of the right-hand side of (3.18a). Of course, the

displacement fields are still same as for the element N3U18. Unfortunately, none of the elements we formulated based on (3.17) or (3.18) shows significant improvement over the original.

3.2. *Hybrid elements for plane strain deformation*

The elements introduced in the last section are based on the principle of minimum potential energy, which requires continuity of first derivatives of the displacements. Consequently, the displacements as well as their first derivatives are used as nodal variables, resulting in large number of degrees of freedom for one element and compromising computational efficiency. Moreover, the shape functions are relatively complicated to formulate. In this section, the following variational statement is used as the basis of an alternative finite element formulation

$$\Pi(\mathbf{u},\boldsymbol{\theta},\boldsymbol{\tau}) = \int_V \left\{ w(\boldsymbol{\varepsilon},\boldsymbol{\chi}) + \frac{1}{2}\kappa\varepsilon_m^2 \right\} \mathrm{d}V + \int_V \tau_{ji}\alpha_{ij}\,\mathrm{d}V - \int_{S_T} (T_i^0 u_i + q_i^0 \theta_i)\,\mathrm{d}S \tag{3.19a}$$

with

$$\delta\Pi(\mathbf{u},\boldsymbol{\theta},\boldsymbol{\tau}) = 0, \tag{3.19b}$$

where τ_{ij} is the anti-symmetric component of the stresses, and

$$\alpha_{ij} = e_{ijk}\theta_k - \tfrac{1}{2}(u_{j,i} - u_{i,j}). \tag{3.20}$$

In (3.19), both the displacements u_i and the rotations θ_i are considered as independent variables. For a couple-stress solid, $\alpha_{ij} = 0$ enforces the relationship between rotations θ_i and displacements u_i. The variational statement (3.19) is derived through enforcing $\alpha_{ij} = 0$ in an averaged sense in (3.1) by use of the Lagrange multipliers τ_{ij}, which are the anti-symmetric stress components. This principle was first used by Herrmann (1983) as the basis for a finite element formulation of couple-stress solids.

Plane strain elements based on (3.19) have as primary dependent variables the displacement components (u, v), the rotation $\theta = \theta_3$, and the anti-symmetric component of the stress $\tau = \tau_{12} = -\tau_{21}$. Within this framework, we have formulated 4-, 6-, 8-, and 9-noded elements. For these elements, there are three nodal values at each nodes, namely (u, v, θ), and one constant τ within each element. Therefore, both displacements and rotations are continuous across elements, but not τ. Figure 3 shows

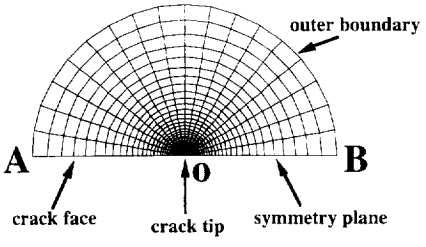

Fig. 4. Finite element mesh for crack tip problem using element N4U13.

such a 4-noded element. Elements with continuous τ have also been explored, but generally performed poorly. The total degrees of freedom for an N-noded elements are thus $(3N+1)$. We shall denote those elements as N4U13, N6U19, N8U25, and N9U28, respectively. These are standard isoparametric elements, with the same shape functions for u, v, and θ. The details of formulation are omitted here for brevity. Numerical quadrature is used, with full integration for the deviatoric part of the strain energy and reduced integration for the volumetric part. The second term in (3.19a), which enforces the rotation–displacement relationship, is also fully integrated, although numerical experiments show little difference if reduced integration were used instead.

All the elements developed above have been used to calculate the plane strain crack tip fields for the strain gradient theory of plasticity given in Section 2. The performance of any of these elements depends strongly on the constitutive parameters, the fineness of the mesh, and the compressibility of the solid. For the power law solid with $n = 5$, all elements behaved quite well if $l = 0$, even for very fine meshes. However, when strain gradient effects come into play ($l > 0$), the performance of all the elements deteriorates to some extent. The best element in terms of performance, accuracy, and economy seems to be the 4-noded N4U13. The results reported in the next section for plane strain crack tip fields are computed using this element, with 18 elements distributed circumferentially around the crack tip in the range $0 < \theta < \pi$. The accuracy of the numerical results are validated by other elements and by internal consistency as the mesh is refined.

4. NUMERICAL RESULTS FOR CRACK TIP FIELDS

Numerical results are presented in this section, obtained using the finite element methods outlined in the last section. Results for the dimensionless quantities in (2.13) are first presented for plane strain mode I, followed by results for mode II. The 4-noded hybrid element N4U13 is used with the mesh shown in Fig. 4. Computations with other elements and other meshes have also been performed to check the accuracy of results that will be presented below. Displacements and rotation are prescribed on the outer boundary coinciding with the HRR solution in (2.12); the functions $\tilde{u}_i$ are taken from Symington *et al.* (1988). The outer radius of the mesh is taken to be $10l$. The numerical results presented below, together with numerical results obtained with meshes having other outer radii, indicate that the choice of $10l$ is adequate. For mode I, $v = \theta = 0$ is enforced on the symmetry plane, while $u = 0$ for the mode II case. The crack flank on $\theta = \pi$ is free of force and moment tractions; these conditions are enforced as natural boundary conditions by the variational principle. All results presented below were computed with $n = 5$, although calculations were also carried out for other values of n.

4.1. *Plane strain mode I crack tip fields*

Distributions of the dimensionless stress components in (2.13), $\hat{\sigma}_{ij}$, $\hat{\tau}_{ij}$, and $\hat{\Sigma}$, are plotted in Fig. 5(a)–(f). The normalized effective stress quantity $\hat{\Sigma}$ is defined in the same manner as the other stresses in (2.13) according to

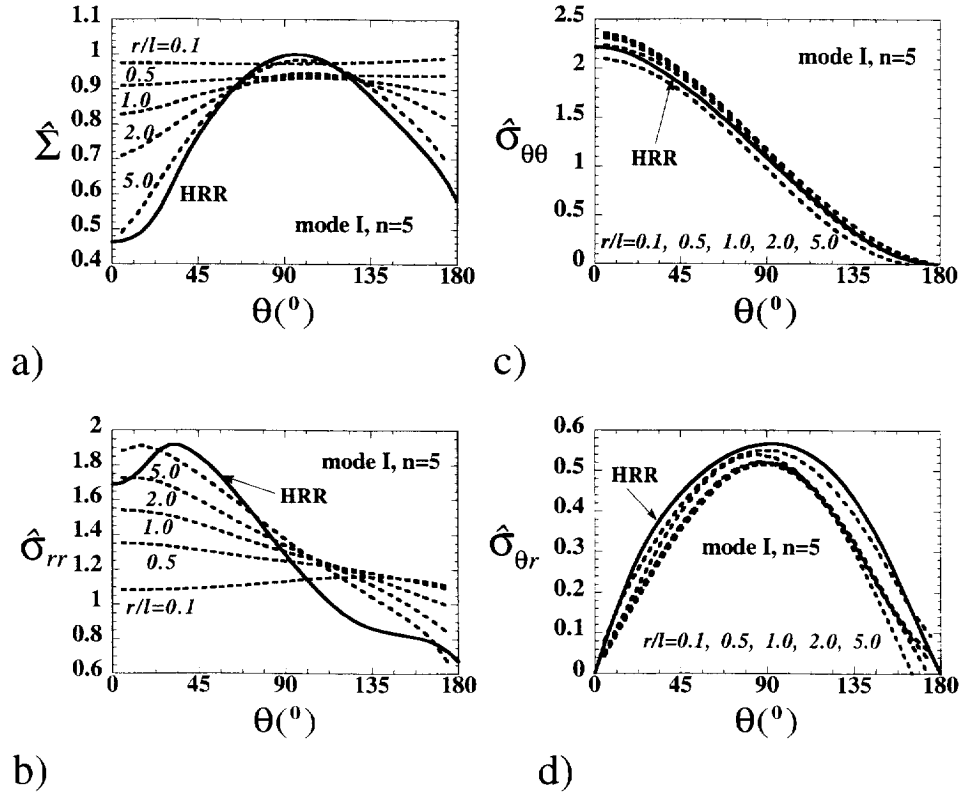

Fig. 5. Distributions of normalized stress components defined in (2.13) and (4.1) for mode I.

$$\Sigma = \sigma_0 \left(\frac{J}{\sigma_0 \varepsilon_0 I_n r} \right)^{1/(n+1)} \hat{\Sigma}\left(\frac{r}{l}, \theta, n \right). \tag{4.1}$$

Included in these plots is the HRR solution, shown as the solid line curves, which with the normalization of (2.13) depends only on θ ($\hat{\tau}_{\theta r}$ vanishes for the classical theory). The computed results for $r/l = 5$ can be seen to be close to the HRR limit. This provides internal consistency indicating that the choice of radius, $r/l = 10$, on which the HRR displacements were prescribed is sufficiently remote from the tip. The plots indicate that gradient effects are strongly evident for $r/l = 1$. Moreover, the trends with r/l give convincing evidence that the dimensionless quantities, $\hat{\sigma}_{ij}$, etc., are bounded as r/l approaches zero. Note especially that the component of the anti-symmetric stress tensor, $\hat{\tau}_{\theta r}$, undergoes little change for r/l decreasing from two orders of magnitude from 0.1 to 0.001.

The stress components $\hat{\sigma}_{\theta\theta}$ and $\hat{\sigma}_{\theta r}$ are surprisingly insensitive to gradient effects according to the present constitutive relation. In particular, the traction on the line directly ahead of the crack tip, $\sigma_{\theta\theta}(\theta = 0)$, is virtually unaffected by the gradient dependence. On the other hand, the effective stress Σ increases by more than a factor

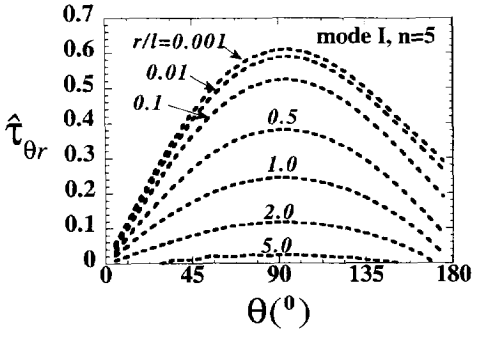

e)

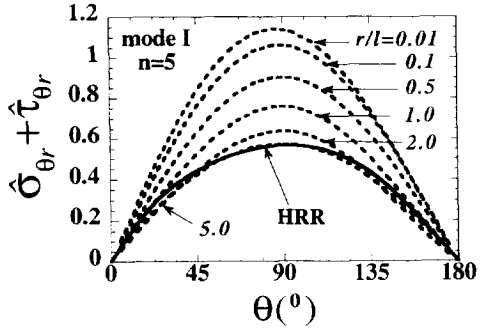

f)

Fig. 5—*Continued.*

of two relative to the effective stress in the HRR solution as r approaches zero. The same is true for the shear traction, $T_r = \sigma_{\theta r} + \tau_{\theta r}$, acting on the radial line emanating from the tip with $\theta = 90°$, due to the contribution of the anti-symmetric stress component. The effective stress Σ becomes independent of θ as the tip is approached, as will be evident from the asymptotic analysis in the next section.

Companion results for the dimensionless strain variations defined in (2.13) are given in the plots of Fig. 6. It will be evident from the results for the singular fields presented in the next section that these strains are associated with irrotational displacements as the tip is approached. To examine the role of the curvatures, χ_{ij}, we have included plots in Fig. 7 of the normalized total effective strain E and the two quantities from which it is composed, the effective strain ε_e and the effective curvature χ_e, at two distances from the tip, $r/l = 1$ and $r/l = 0.01$. The effective strain ε_e makes the dominant contribution to the total strain E, and it will be argued in the next section that $l\chi_e$ is less singular than ε_e as r/l approaches zero. (This is more evident from the numerical results for mode II, as can be seen by looking ahead to Fig. 10.) The effective strain ε_e immediately ahead of the tip on $\theta = 0$ is significantly larger than the corresponding strain predicted by the HRR solution. Thus, one of the main

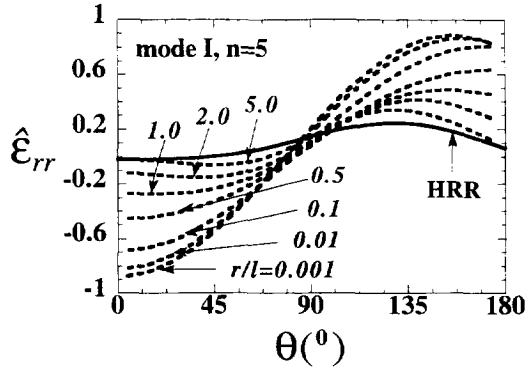

a)

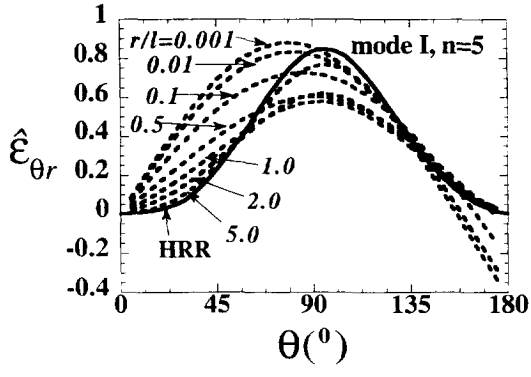

b)

Fig. 6. Distributions of normalized strain components defined in (2.13) for mode I.

distinctions between the predictions of the two theories is the substantial enhancement of both Σ and ε_e ahead of the crack tip in the strain gradient solution relative to the HRR solution. This distinction exists even though the traction on the plane ahead of the tip is nearly the same in the two solutions.

4.2. *Plane strain mode II crack tip fields*

Arguments concerning the relative order of the singular contributions apply for the mode II problem as well. Equation (2.13) pertains with the non-dimensional quantities topped by the circumflex being bounded as r/l approaches zero and approaching the corresponding quantities in (2.12) for r/l large. The displacements from the HRR solution in (2.12) are prescribed on $r/l = 10$.

Stress components are presented in Fig. 8(a)–(f). As in mode I, the components of the symmetric stress tensor depart only modestly from the HRR solution. The effective stress Σ becomes independent of θ as r approaches zero. The major difference between the predictions of the two theories in mode II is the magnitude of the shear traction,

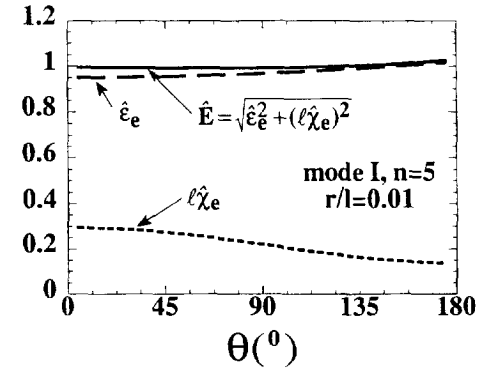

a)

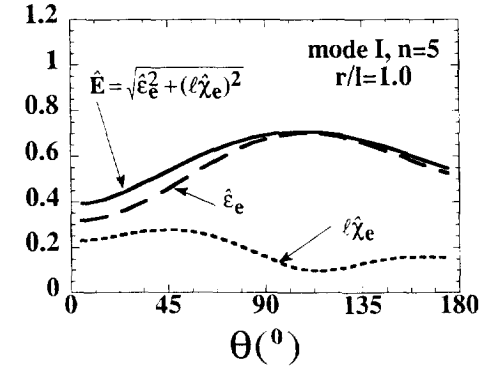

b)

Fig. 7. Distributions of the total effective strain E and the two quantities from which it derives for mode I at (a) $r/l = 0.01$ and (b) $r/l = 1$.

$\sigma_{\theta r}+\tau_{\theta r}$, directly ahead of the crack tip, which is larger by more than a factor of two relative to the HRR solution. Here, again, this is almost entirely due to the contribution from the anti-symmetric stress component $\tau_{\theta r}$.

Strain distributions are plotted in Figs 9 and 10. The strains approach the distributions is given later in Section 5.2 for mode II for small r/l. The contribution of $l\chi_e$ to the total strain E is largest when r/l is about unity and approaches zero as the tip is approached, as seen in Fig. 10. It is seen again that E becomes independent of θ near the tip. Relative to the HRR solution, the strain gradient theory predicts strains ahead of the tip that are lower by a factor of two while the shear tractions are larger by a factor of more than two.

5. DOMINANT SINGULAR FIELDS

For the present constitutive theory with $n > 1$, Huang *et al.* (1995) concluded that it is not possible to have a dominantly singular solution of separable form with ε_{ij} and

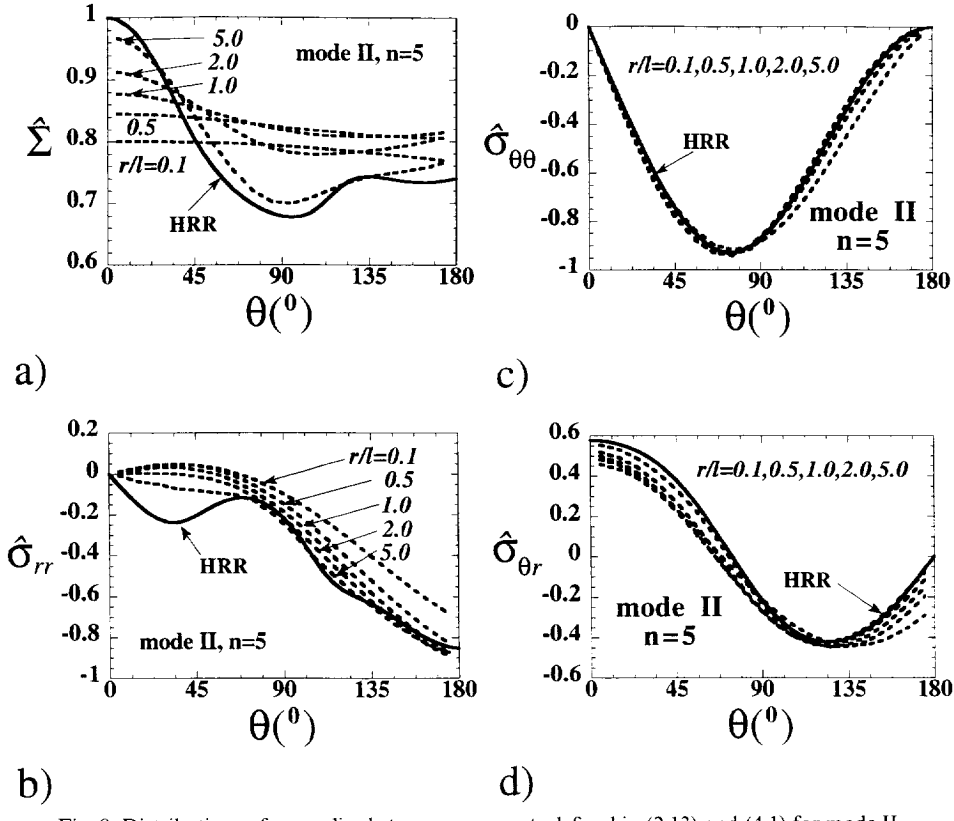

Fig. 8. Distributions of normalized stress components defined in (2.13) and (4.1) for mode II.

χ_{ij} having the same singular dependence on r, and we corroborate that finding in the Appendix. The numerical results presented in Section 4 give strong evidence for the dominance of the strains over the curvatures, χ_{ij}. As already noted, this is only possible if the dominant displacement field is irrotational. Our starting point will be to look for a dominant singular solution derived from an incompressible, irrotational displacement field.

5.1. *Mode I*

It is readily verified that the only mode I strain distribution varying in accord with $r^{-n/(n+1)}$ and derived from an incompressible, irrotational displacement field is specified by

$$(\hat{\varepsilon}_{rr}, \hat{\varepsilon}_{r\theta}) = A\left(-\cos\left(\frac{n+2}{n+1}\theta\right), \sin\left(\frac{n+2}{n+1}\theta\right)\right), \tag{5.1}$$

where $\hat{\varepsilon}_{\theta\theta} = -\hat{\varepsilon}_{rr}$, A is a positive amplitude factor to be determined, and the nor-

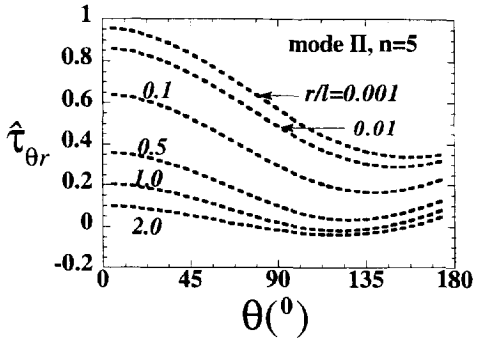

e)

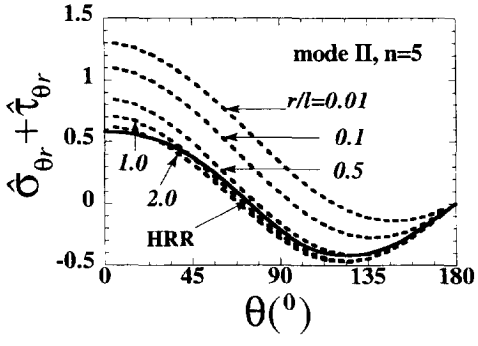

f)

Fig. 8—*Continued.*

malization introduced in (2.13) is retained. The effective strain from (5.1) is independent of θ and given by

$$\varepsilon_e = \varepsilon_0 \left(\frac{J}{\sigma_0 \varepsilon_0 I_n r} \right)^{n/(n+1)} \frac{2}{\sqrt{3}} A. \tag{5.2}$$

The effective stress σ_e is also independent of θ, and it is straightforward to show that

$$(\hat{s}_{rr}, \hat{s}_{r\theta}) = \frac{1}{\sqrt{3}} \left(\frac{2A}{\sqrt{3}} \right)^{1/n} \left(-\cos\left(\frac{n+2}{n+1} \right)\theta, \sin\left(\frac{n+2}{n+1} \right)\theta \right) \tag{5.3}$$

subject to the normalization (2.13). In planar polar coordinates, the first set of equilibrium equations in (2.10) is

$$\begin{aligned} \sigma_{rr,r} + r^{-1}(\sigma_{r\theta,\theta} - \tau_{r\theta,\theta}) + r^{-1}(\sigma_{rr} - \sigma_{\theta\theta}) &= 0, \\ \sigma_{r\theta,r} + \tau_{r\theta,r} + r^{-1}\sigma_{\theta\theta,\theta} + 2r^{-1}\sigma_{r\theta} &= 0. \end{aligned} \tag{5.4}$$

With $\sigma_m = \sigma_{kk}/3$ as the mean stress, write

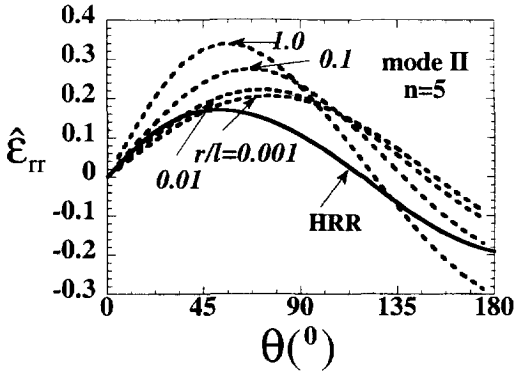

a)

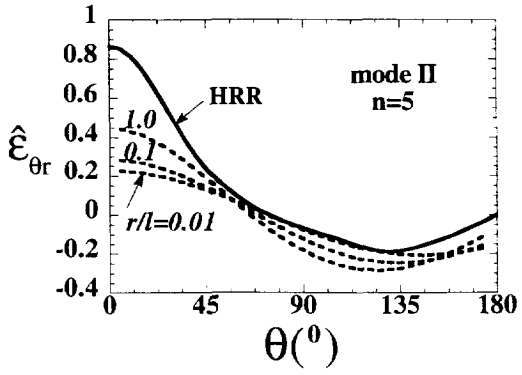

b)

Fig. 9. Distributions of normalized stress components defined in (2.13) for mode II.

$$(\sigma_m, \tau_{r\theta}) = \sigma_0 \left(\frac{J}{\sigma_0 \varepsilon_0 I_n r} \right)^{1/(n+1)} (\hat{\sigma}_m, \hat{\tau}_{r\theta}) \quad \text{with} \quad (\hat{\sigma}_m, \hat{\tau}_{r\theta}) = \frac{1}{\sqrt{3}} \left(\frac{2A}{\sqrt{3}} \right)^{1/n} (f(\theta), g(\theta)). \tag{5.5}$$

Noting that $\sigma_{rr} = s_{rr} + \sigma_m$ and $\sigma_{\theta\theta} = s_{\theta\theta} + \sigma_m$, one can reduce (5.4) to

$$\frac{dg}{d\theta} + \frac{1}{(n+1)} f = -\frac{(n-1)}{(n+1)} \cos\left(\frac{n+2}{n+1} \theta \right),$$

$$\frac{df}{d\theta} - \frac{1}{(n+1)} g = -\frac{(n-1)}{(n+1)} \sin\left(\frac{n+2}{n+1} \theta \right). \tag{5.6}$$

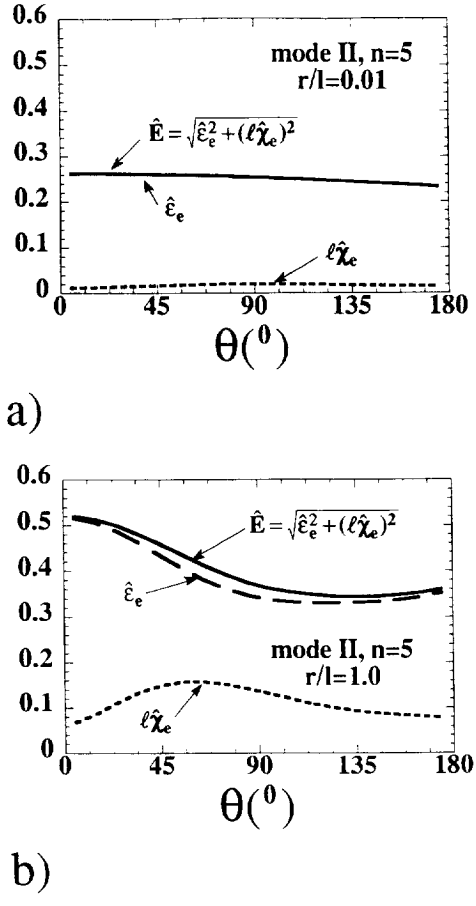

Fig. 10. Distributions of the total effective strain E and the two quantities from which it derives for mode II at (a) $r/l = 0.01$ and (b) $r/l = 1$.

The solution to (5.6), subject to mode I symmetry and the vanishing of both $\hat{\sigma}_{\theta\theta}$ and $\hat{\sigma}_{\theta r}+\hat{\tau}_{\theta r}$ at $\theta = \pi$ is

$$f=\frac{2n}{n+1}\cos\left(\frac{1}{n+1}\theta\right)+\frac{n-1}{n+1}\cos\left(\frac{n+2}{n+1}\theta\right)$$

$$\text{and}\quad g=-\frac{2n}{n+1}\sin\left(\frac{1}{n+1}\theta\right)-\frac{n-1}{n+1}\sin\left(\frac{n+2}{n+1}\theta\right). \tag{5.7}$$

The stresses and strains associated with the dominantly singular field have now been fully determined apart from the amplitude factor A. Evaluation of the J-integral expression in (2.11) using these fields gives (after a fairly lengthy, but relatively straightforward, calculation)

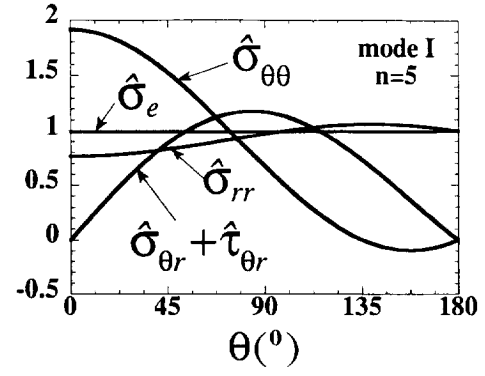

a)

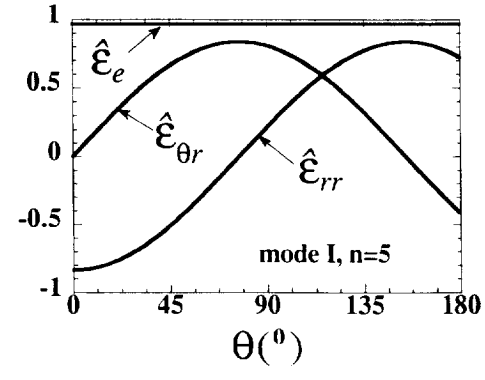

b)

Fig. 11. Distributions of normalized stresses and strains for mode I with $n = 5$ for the singular solution of Section 5.

$$A = \frac{\sqrt{3}}{2}\left(\frac{n+1}{2n\pi} I_n\right)^{n/(n+1)}. \tag{5.8}$$

In summary, the normalized θ-variations of the strains are given by (5.1) and the corresponding stress variations ($\hat{\sigma}_{\theta\theta}, \hat{\sigma}_{rr}, \hat{\sigma}_{r\theta}, \hat{\tau}_{r\theta}$) are given by (5.3) and (5.5) where $\hat{\sigma}_{\theta\theta} = \hat{s}_{\theta\theta} + \hat{\sigma}_m$ and $\hat{\sigma}_{rr} = \hat{s}_{rr} + \hat{\sigma}_m$. Plots of the normalized stresses and strains from these equations for $n = 5$ are given in Fig. 11. Comparison of these variations with the numerical solutions given in the previous figures leaves little doubt that the irrotational singular fields produced in this section are the desired asymptotic singular crack tip fields.

A further simplification is achieved if the HRR factor I_n is eliminated, thereby directly linking the near-tip quantities with J. Using (5.8) with (2.13), one finds

$$[\sigma_{\theta\theta}, \sigma_{rr}, \sigma_{\theta r}+\tau_{\theta r}] = \frac{2n\sigma_0}{\sqrt{3}(n+1)}\left(\frac{(n+1)J}{2n\pi\sigma_0\varepsilon_0 r}\right)^{1/(n+1)} \times \left[\cos\left(\frac{n+2}{n+1}\theta\right)+\cos\left(\frac{1}{n+1}\theta\right)\right.$$
$$\left. -\frac{1}{n}\cos\left(\frac{n+2}{n+1}\theta\right)+\cos\left(\frac{1}{n+1}\theta\right), \sin\left(\frac{n+2}{n+1}\theta\right)+\sin\left(\frac{1}{n+1}\theta\right),\right. \quad (5.9a)$$

$$[\varepsilon_{rr}, \varepsilon_{\theta r}, \varepsilon_e] = \varepsilon_0\left(\frac{(n+1)J}{2n\pi\sigma_0\varepsilon_0 r}\right)^{n/(n+1)} \times \left[-\frac{\sqrt{3}}{2}\cos\left(\frac{n+2}{n+1}\theta\right), \frac{\sqrt{3}}{2}\sin\left(\frac{n+2}{n+1}\theta\right), 1\right]. \quad (5.9b)$$

Apart from a free amplitude factor, these singular stresses and strains agree with those found by Huang *et al.* (1995) for their version of the present constitutive law which combines ε_e and χ_e into the single total effective strain E in a different manner from (2.1). Their asymptotic analysis produces two amplitude factors, one proportional to the present A controlling the irrotational field and the second multiplying the couple stresses. Each makes a contribution to J which cannot be determined by the asymptotic analysis alone. If the second amplitude factor is set to zero ($A^{(0)} = 0$ in their notation), their singular fields should coincide precisely with (5.9), in spite of the difference in the two constitutive assumptions. A comparison of the two sets of results shows that this is indeed the case.

The limit $n = 1$ is special in the sense that it is possible to have a dominant singular field with both ε_{ij} and χ_{ij} having the same $r^{-1/2}$ singularity (c.f. Appendix). The constitutive model of Huang *et al.* (1995) coincides with the present model for $n = 1$, and these authors have shown that there are two amplitude factors in this limit, with one constraint provided by J. Thus, the expressions in this section for the singular stresses and strains do not necessarily apply for $n = 1$.

5.2. *Mode II*

The analysis for mode II follows along precisely the lines outlined above for mode I. The results are as follows. The normalized quantities defined in (2.13) are found to be

$$[\hat{\varepsilon}_{rr}, \hat{\varepsilon}_{\theta r}, \hat{\varepsilon}_e] = \left(\frac{(n+1)I_n}{2n\pi}\right)^{n/(n+1)}\left[\frac{\sqrt{3}}{2}\sin\left(\frac{n+2}{n+1}\theta\right), \frac{\sqrt{3}}{2}\cos\left(\frac{n+2}{n+1}\theta\right), 1\right] \quad (5.10a)$$

$$[\hat{\sigma}_{\theta\theta}, \hat{\sigma}_{rr}, \hat{\sigma}_{r\theta}, \hat{\tau}_{r\theta}] = \frac{2n}{\sqrt{3}(n+1)}\left(\frac{(n+1)I_n}{2n\pi}\right)^{1/(n+1)}$$
$$\times \left[-\sin\left(\frac{n+2}{n+1}\theta\right)-\sin\left(\frac{1}{n+1}\theta\right), \frac{1}{n}\sin\left(\frac{n+2}{n+1}\theta\right)\right.$$
$$\left. -\sin\left(\frac{1}{n+1}\theta\right), \frac{n+1}{2n}\cos\left(\frac{n+2}{n+1}\theta\right), -\frac{n-1}{2n}\cos\left(\frac{n+2}{n+1}\theta\right)-\cos\left(\frac{1}{n+1}\theta\right)\right] \quad (5.10b)$$

where I_n is now the normalization factor for the mode II plane strain problem.

The expressions for the dominantly singular strains and stresses with I_n eliminated are

$$[\varepsilon_{rr}, \varepsilon_{\theta r}, \varepsilon_e] = \varepsilon_0 \left(\frac{(n+1)J}{2n\pi\sigma_0\varepsilon_0 r}\right)^{n/(n+1)} \left[\frac{\sqrt{3}}{2}\sin\left(\frac{n+2}{n+1}\theta\right), \frac{\sqrt{3}}{2}\cos\left(\frac{n+2}{n+1}\theta\right), 1\right] \quad (5.11a)$$

$$[\sigma_{\theta\theta}, \sigma_{rr}, \sigma_{\theta r} + \tau_{\theta r}] = \frac{2n\sigma_0}{\sqrt{3}(n+1)} \left(\frac{(n+1)J}{2n\pi\sigma_0\varepsilon_0 r}\right)^{1/(n+1)} \times \left[-\sin\left(\frac{n+2}{n+1}\theta\right) - \sin\left(\frac{1}{n+1}\theta\right), \right.$$
$$\left. \frac{1}{n}\sin\left(\frac{n+2}{n+1}\theta\right) - \sin\left(\frac{1}{n+1}\theta\right), \cos\left(\frac{n+2}{n+1}\theta\right) + \cos\left(\frac{1}{n+1}\theta\right)\right]. \quad (5.11b)$$

6. DISCUSSION

It is remarkable that the dominant singular fields can be obtained in closed form for the present plasticity theory, while the θ-dependence of the plane strain HRR fields can only be obtained numerically for the less complicated J_2 deformation theory. The numerical solutions in Figs 5–10 show that the transition from the HRR fields to the dominant singular solutions occurs smoothly. Roughly speaking, the HRR fields are accurate for $r > 5l$, the singular fields become reasonably accurate for $r < l/5$, and a gradual transition region lies between. The singularity is robust in the sense that it governs behavior within a non-negligible portion of the zone within which strain gradient effects are important.

6.1. *Applicability of the small strain solution*

The solution was derived within the framework of small strain theory. To gain some insight into the range of applicability of the results, direct attention to mode I and consider the effective strain from (2.13)

$$\varepsilon_e = \varepsilon_0 \left(\frac{J}{\sigma_0\varepsilon_0 I_n r}\right)^{n/(n+1)} \hat{\varepsilon}_e. \quad (6.1)$$

As a condition for validity of a small strain solution to within a distance $l/10$ of the crack tip, require that $\varepsilon_e \leqslant 1/10$. It then follows from (6.1) that the crack tip intensity J must satisfy

$$J \leqslant \sigma_0 l \frac{I_n}{100}\left(\frac{1}{10\varepsilon_0}\right)^{1/n}, \quad \hat{\varepsilon}_e^{(n+1)/n} \cong 0.063\sigma_0 l\left(\frac{1}{10\varepsilon_0}\right)^{1/n}, \quad (6.2)$$

where the last estimate uses the value of $\hat{\varepsilon}_e$ from Fig. 7, $n = 5$ and $I_n \cong 5$. As an illustration, if one takes $l = 4$ μm (c.f. Fleck *et al.*, 1994) and $\varepsilon_0 = 0.003$, then J must be less than about 50 J m^{-2} if $\sigma_0 = 100$ MPa and less than 250 J m^{-2} if $\sigma_0 = 500$ MPa. Such levels of J greatly exceed the atomistic work of fracture for metals, which are typically of the order of several J m^{-2}. On the other hand, these levels are below the values of J at crack initiation for some of the toughest metal–ceramic interfaces and

metal crystals undergoing atomic decohesion shielded by a plastic zone. It is also useful to re-express condition (6.2) in terms of the crack tip opening displacement. Using the conventional estimate for the tip opening displacement in plane strain mode I, $J(2\sigma_0)$, one finds

$$\delta_t \leqslant 0.031 l \left(\frac{1}{10\varepsilon_0}\right)^{1/n}. \tag{6.3}$$

Typically, this condition required δ_t to be less than $l/16$, which suggests that the criterion stated above may be unduly restrictive. Finally, it should be noted that the criterion has been derived for a stationary crack. Strains at the tip of an advancing crack are distinctly smaller than those of a stationary crack, and this should also permit the criterion to be relaxed.

6.2. *Implications for fracture and avenues for further research*

The strain gradient theory gives rise to higher stresses near the tip than the conventional theory, but perhaps not as large as might be expected. In particular, the normal stress acting on the plane ahead of a mode I crack tip is largely unaffected by the strain gradient effects considered in this paper. The greatest change occurs for a mode II crack for which the shear traction on the plane ahead of the tip is increased by more than a factor of two relative to the prediction of the conventional theory. As noted in Section 5, the deformations producing the most singular strains and symmetric stresses are irrotational and, therefore, have $\tau_e = 0$. By virtue of the constitutive law used in the present theory, based on (2.1), the expected higher stresses do not occur in mode I. In other words, the most singular deformations adjust to reduce the associated gradient effect. Similar behavior was observed by Fleck and Hutchinson (1993) in their analysis of void growth within the context of the present theory. The dominant deformation mode for a spherical void is a spherically symmetric expansion field which is irrotational. Thus the dominant mode does not contribute to the gradient measure χ_e, with the result that void growth is not significantly influenced according to the present gradient theory. In both instances, the absence of a stronger effect is a consequence of the restricted form of the constitutive law invoked in (2.1) and (2.2), which brings in the gradients only through the one measure χ_e.

An attractive general formulation for isotropic solids dependent on first-order strain gradients has been laid out by Smyshlyaev and Fleck (1995), who extended developments of Mindlin (1965). For incompressible solids, there are three independent invariants of degree two of the second-order displacement gradient tensor, $\eta_{ijk} = u_{k,ij}$. Smyshlyaev and Fleck have shown that η_{ijk} can be decomposed into three measures, $\boldsymbol{\eta} = \boldsymbol{\eta}^{(1)} + \boldsymbol{\eta}^{(2)} + \boldsymbol{\eta}^{(3)}$, which are mutually orthogonal in the sense that $\eta^{(1)}_{ijk}\eta^{(2)}_{ijk} = 0$, etc. then $\eta^{(m)}_{ijk}\eta^{(m)}_{ijk}$ for $m = 1$, 2, and 3 represent three independent invariants. In terms of these invariants, a generalization of (2.1) is

$$E^2 = \varepsilon_e^2 + l^2_{(1)}\eta^{(1)}_{ijk}\eta^{(1)}_{ijk} + l^2_{(2)}\eta^{(2)}_{ijk}\eta^{(2)}_{ijk} + l^2_{(3)}\eta^{(3)}_{ijk}\eta^{(3)}_{ijk} \tag{6.4}$$

involving three non-negative material length parameters, $l_{(i)}$. One of the strain gradient terms in (6.4) can be normalized such that it coincides with $l^2\chi_e^2$. Thus, with the other

two length parameters set to zero, (6.4) reduces to the relation (2.1) used as the basis of the present work. With all three length parameters as positive, (6.4) is positive such that any non-zero strain gradient will give rise to a non-zero E. The irrotational displacement field associated with the dominant stresses and strains at the crack tip found in the present study would be excluded if the constitutive law were based on (6.4) with at least two of the three length parameters being non-zero. It is likely that the near tip stresses for a solid based on the more general total strain measure (6.4) would be higher than those based on (2.1), perhaps significantly so.

Further effort will be required to understand the relationship between crack tip stresses and constitutive behavior in the regime near the tip where strain gradients become important. The present results for the pure mode I and mode II fields in plane strain have been derived for a limited class of solids whose dependence on strain gradients is through the single invariant χ_e. As discussed above, this model may miss significant aspects of strain gradient dependence. Of equal importance is the need to establish fundamental connections between phenomenological total strain measures used to formulate the constitutive law, such as (2.1) and (6.4), and dislocation patterns associated with strain gradient deformations.

ACKNOWLEDGMENTS

This work was partially supported by the U.S. Office of Naval Research under Grant N00014-92-J-1960, by the National Science Foundation under Grant MSS-92-02141, and by the Division of Applied Sciences, Harvard University. The authors are grateful for many helpful discussions with Dr Norman A. Fleck of Cambridge University. The authors also acknowledge a most helpful interaction with Drs Young Huang and Keh-Chih Hwang who made their paper on the analytical solution for the dominant singular fields available to us after a first draft of our paper was prepared. Section 5 of the present paper was added subsequently with the insight gained from this paper.

REFERENCES

Cowper, G. R. (1973) Gaussian quadrature formulas for triangles. *Int. J. Numer. Mech. Engng* **7**, 405–408.

Cosserat, E. and Cosserat, F. (1909) *Theorie des Corps Deformables*. Herman et fils, Paris.

de Borst, R. (1993) A generalisation of J_2-flow theory for polar continua. *Comput. Methods Appl. Mech. Engng* **103**, 347–362.

Fleck, N. A. and Hutchinson, J. W. (1993) A phenomenological theory for strain gradient effects in plasticity. *J. Mech. Phys. Solids* **41**, 1825–1857.

Fleck, N. A., Muller, G. M., Ashby, M. F. and Hutchinson, J. W. (1994) Strain gradient plasticity: theory and experiment. *Acta Metall. Mater.* **42**, 475–487.

Herrmann, L. R. (1983) Mixed finite elements for Couple-stress analysis. In *Hybrid and Mixed Finite Element Methods* (ed. S. N. Atluri, R. H. Gallagher and O. C. Zienkiewicz). John Wiley & Sons Ltd.

Huang, Y., Zhang, L., Guo, T. F. and Hwang, K. C. (1995) Near-tip fields for cracks in materials with strain gradient effects, to be published in the Proceeding of the IUTAM Symposium on Nonlinear Fracture Mechanics held at Cambridge University, 3–7 September, 1995.

Hutchinson, J. W. (1968) Singular behavior at the end of a tensile crack in a hardening material. *J. Mech. Phys. Solids* **16,** 13–31.
Koiter, W. T. (1964) Couple stresses in the theory of elasticity, I and II. *Proc. Ned. Akad. Wet. (B)* **67**(1), 17–44.
Ma, Q. and Clarke, D. R. (1995) Size dependent hardness of silver single crystals, to be published in *J. Mater. Res.*
Mindlin, R. D. (1965) Second gradient of strain and surface tension in linear elasticity. *Int. J. Solids Struct.* **1,** 417–438.
Poole, W. J., Ashby, M. R. and Fleck, N. A. (1995) Micro-hardness of annealed and work-hardened copper polycrystals, to be published in *Acta Metall. Mater.*
Rice, J. R. (1968) A path-independent integral and the approximate analysis of strain concentration by notches and cracks. *J. Appl. Mech.* **35,** 379–386.
Rice, J. R. and Rosengren, G. F. (1968) Plane strain deformation near a crack tip in a power law hardening material. *J. Mech. Phys. Solids* **16,** 1–12.
Shiermeier, A. D. (1996) In preparation.
Simo, J. C., Taylor, R. L. and Pister, K. S. (1985) Variational and projection methods for the volume constraint in finite deformation elasto-plasticity. *Comp. Meths. Appl. Mech. Engng* **51,** 177–208.
Smyshlyaev, V. P. and Fleck, N. A. (1995) The role of strain gradients in the grain size effect for polycrystals, submitted for publication.
Stelmashenko, N. A., Walls, M. G., Brown, L. M. and Milman, Yu. V. (1993) Micro-indentations on W and Mo oriented single crystals: an STM study. *Acta Metall. Mater.* **41,** 2855–2865.
Symington, M., Shih, C. F. and Ortiz, M. (1988) Tables of plane strain mixed-mode plastic crack tip fields. Brown University Technical Report, October.
Specht, B. (1988) Modified shape functions for the three node plate bending element passing the patch test. *Int. J. Numer. Meth. Engng* **26,** 705–715.
Zienkiewicz, O. C. and Taylor, R. L. (1989a) *The Finite Element Method, Vol. 1: Basic Formulation and Linear Problems*, 4th edn. McGraw-Hill, London.
Zienkiewicz, O. C. and Taylor, R. L. (1989b) *The Finite Element Method, Vol. 2: Solid and Fluid Mechanics, Dynamics and Non-Linearity*, 4th edn. McGraw-Hill, London.

APPENDIX: ANALYSIS OF COUPLED SINGULAR FIELDS

We look for dominantly singular fields where both ε_{ij} and χ_{ij} behave as $r^{-n/(n+1)}$ as r approaches zero. The discussion will focus on the plane strain, mode I problem. As already discussed, such coupled fields would only be possible in separable form if

$$(u_r, u_\theta) = A(n+1)r^{1/(n+1)}\left(-\cos\left(\frac{n+2}{n+1}\theta\right), \sin\left(\frac{n+2}{n+1}\theta\right)\right) + r^{(n+2)/(n+1)}\left(-\frac{n+1}{2n+3}u'(\theta), u(\theta)\right), \tag{A.1}$$

where the first contribution with amplitude A is irrotational and the second gives rise to non-zero χ_{ij}. Both contributions are incompressible. The function $u(\theta)$ is to be determined. A prime denotes differentiation with respect to θ. The rotation from (A.1) is

$$\theta_3 = r^{1/(n+1)}\frac{1}{2}\left(\frac{n+1}{2n+3}u'' + \frac{2n+3}{n+1}u\right) \equiv r^{1/(n+1)}\omega(\theta). \tag{A.2}$$

A direct calculation shows that

$$E = \sqrt{\varepsilon_e^2 + l^2\chi_e^2} = r^{-n/(n+1)}\sqrt{4A^2/3 + l^2\chi(\theta)^2} \equiv r^{-n/(n+1)}\tilde{E}(\theta), \tag{A.3}$$

where $\chi(\theta) = \sqrt{2(\omega'^2 + (\omega/(n+1))^2)/3}$. The moment equilibrium equation in (2.10) can only be satisfied to lowest order by the coupled fields if $e_{ijk}m_{pi,p} = 0$. In planar polar coordinates, this equation is $(rm_{r3})_{,r} + m_{\theta 3,\theta} = 0$. When the couple stresses are expressed in terms of χ_{3r} and $\chi_{3\theta}$ with the aid of the constitutive equation and then in terms of ω and ω', the moment equilibrium equation can be reduced to a non-linear second-order ordinary differential equation for $\omega(\theta)$

$$(\tilde{E}^{-(n-1)/n}\omega')' + \frac{n}{(n+1)^2}\tilde{E}^{-(n-1)/n}\omega = 0. \tag{A.4}$$

Further reduction of this equation using (A.3) and the definition of $\chi(\theta)$ gives

$$\omega'' + \frac{2[n(n+1)(A/l)]^2 + [(n^2-1)^2 + n(n+1)^2]\omega'^2 + n^2\omega^2}{(n+1)^2[2n(n+1)^2(A/l)^2 + (n+1)^2\omega'^2 + n\omega^2]}\omega = 0. \tag{A.5}$$

Symmetry and the boundary condition $m_{\theta 3}$ at $\theta = \pi$ require

$$\omega(0) = 0 \quad \text{and} \quad \omega'(\pi) = 0. \tag{A.6}$$

For $n = 1$, (A.5) with (A.6) is satisfied by $\omega = c\sin(\theta/2)$ for all values of A. Coupled solutions of the type sought are possible in this limit, and such solutions have been considered by Huang *et al.* (1995).

For $n > 1$, we have explored the possibility of solutions to (A.5) with (A.6) using a simple numerical shooting procedure. Without loss of generality, one can take $\omega(0) = 0$ and $\omega'(0) = 1$, and integrate across the interval to obtain $\omega'(\pi)$. Note that (A.5) is well conditioned—both the numerator and the denominator in the term multiplying ω are positive if $A > 0$. A solution exists for each n if $A = 0$. This confirms the finding of Huang *et al.* (1995) who used a stress-based formulation to carry out their analysis. If $n > 1$, no solutions were found for any $a > 0$, again verifying the findings of Huang *et al.* in their analysis of the present version of the constitutive model. The conclusion for $n > 1$ is that no coupled solution of the type sought exists. The numerical results in the body of the paper give strong support to the existence of dominantly singular fields which are irrotational with less singular couple stresses and curvatures.